

Assimilation of GIRO data into a real-time IRI

I. A. Galkin,¹ B. W. Reinisch,^{1,2} X. Huang,¹ and D. Bilitza³

Received 30 November 2011; revised 24 February 2012; accepted 1 March 2012; published 17 April 2012.

[1] Increasingly accurate and detailed global 3-D specification of the Earth's space plasma environment is required to further understand its intricate organization and behavior. For a long time space physics and aeronomy research has been data starved due to the great variety of natural time scales involved in the plasma phenomenology. We have started developing a new approach to the global ionospheric specification called Real-Time Assimilative Mapping (RTAM). The IRI-RTAM will use data from the Global Ionospheric Radio Observatory (GIRO) to smoothly transform IRI's background empirical maps of the ionospheric characteristics to match the observations. Such empirical assimilative modeling will provide a high-resolution, global picture of the ionospheric response to various short-term events observed during periods of storm activity or the impact of gravity waves coupling the ionosphere to the lower atmosphere, including timelines of the vertical restructuring of the plasma distribution. It will also contribute to the challenging task of providing a rapid insight into the temporal and spatial space weather development using the real-time GIRO data streams. The new assimilation technique "updates" the IRI electron density distribution while preserving the overall integrity of IRI's typical ionospheric feature representations. The technique adjusts the coefficients of the spherical/diurnal expansions used by the CCIR and URSI-88 model to obtain the global subpeak electron density distribution. The set of global corrected coefficients can be generated as frequently as every 15 min and easily disseminated using a single real-time RTAM server operated by GIRO.

Citation: Galkin, I. A., B. W. Reinisch, X. Huang, and D. Bilitza (2012), Assimilation of GIRO data into a real-time IRI, *Radio Sci.*, 47, RS0L07, doi:10.1029/2011RS004952.

1. Introduction

[2] Conventional wisdom has long held that an empirical model that represents an average essence of the measurement data will have limited success in describing the variety of short-term events and predict how system will respond to them. The ionospheric forecasting community therefore, has been focusing on the development of comprehensive theoretical models that assimilate real-time sensor data, following a similar process that was successfully applied in describing terrestrial weather. Meanwhile, the computational ease of empirical models made them readily available to the wide audience of space physics and radio wave propagation communities. The International Reference Ionosphere (IRI) empirical model with a long history of development and refinement [Rawer *et al.*, 1978; Bilitza, 1990, 2001; Bilitza and Reinisch, 2008] has been used for a wide range of applications in science, engineering, and education and has generally outperformed other empirical and theoretical

models. This was again shown in recent event-based comparisons of ionospheric models with ground and space measurements in the framework of the CEDAR Electrodynamics Thermosphere Ionosphere (ETI) Challenge by the Community Coordinated Modeling Center (CCMC) where IRI was one of the two top performers [Shim *et al.*, 2010], the other being the Utah State University Global Assimilation of Ionospheric Measurements (USU-GAIM) model, a theoretical model that assimilates a diverse set of measured data [Scherliess *et al.*, 2006].

[3] The next challenge for IRI is to employ data assimilative capabilities to further its proven performance to ionospheric conditions far from an average quiet time behavior. First attempts toward this goal were made by Bilitza *et al.* [1997] with ionosonde data, and by Komjathy *et al.* [1998] and Hernandez-Pajares *et al.* [2002] with GPS TEC data. This paper describes the roadmap to building a real-time extension of the IRI based on an *assimilative modeling* approach called Real-Time Assimilative Mapping (RTAM). The IRI-RTAM approach will initially use data from the Global Ionospheric Radio Observatory (GIRO) [Reinisch and Galkin, 2011], whose sensor locations are shown in Figure 1, to smoothly transform IRI's climatologic maps of the ionospheric characteristics so that they match the observations. On one hand, RTAM is based on the *empirical* background model formalism that is not

¹Center for Atmospheric Research, University of Massachusetts Lowell, Lowell, Massachusetts, USA.

²Lowell Digisonde International, LLC, Lowell, Massachusetts, USA.

³Space Weather Laboratory, George Mason University, Fairfax, Virginia, USA.

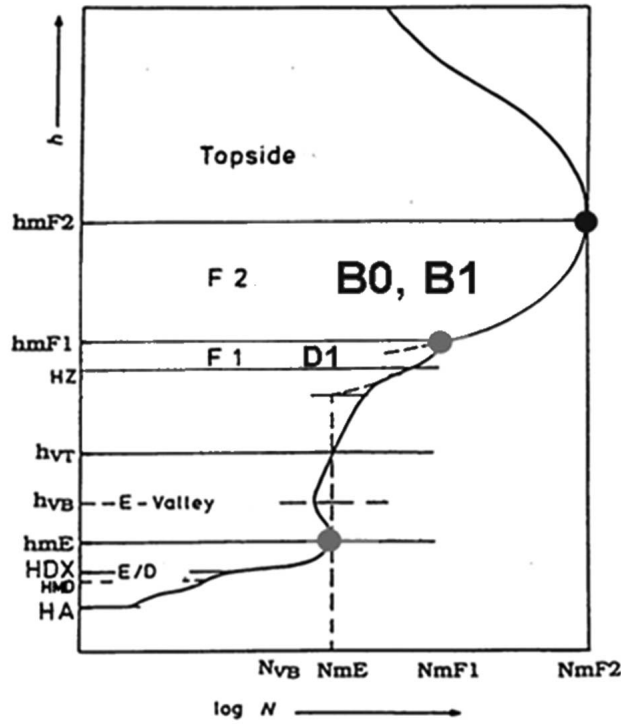


Figure 2. The electron density profile of the IRI model [Bilitza, 1990] is based on world maps for monthly median characteristics, including peak densities and heights of the F2 layer (black dot) and F1 and E layers (gray dots).

representation for any given location is written as a spatial expansion over the latitude λ and longitude θ :

$$A_i(\lambda, \theta) = \sum_{n=0}^{75} U_{in} G_n(\lambda, \theta), \quad (2)$$

where $G_n(\lambda, \theta)$ are 2-D geographic coordinate functions used as the spatial expansion basis. Though frequently called “spherical harmonic functions” in the ionospheric literature, $G_n(\lambda, \theta)$ are only similar in their formulation to the classic surface spherical harmonics that arise naturally in physical problems with spherical symmetry [e.g., Hobson, 1931]. The zonal dimension of the $G_n(\lambda, \theta)$ basis functions is actually expressed as a conventional 8 degree harmonic expansion over geographic longitude θ to optimally represent the day/night dependence of f_oF2 :

$$A_i(\lambda, \theta) = \sum_{j=0}^{J(0)} C_{ij0} P_{j0}(\lambda, \theta) + \sum_{k=1}^8 \sum_{j=0}^{J(k)} (C_{ij2k-1} \cos k\theta + C_{ij2k} \sin k\theta) P_{jk}(\lambda, \theta) \quad (3)$$

[7] However, the meridional dimension of the spherical expansion does not use the traditional Legendre definition, but rather a custom power function that captures, in addition to the solar-controlled geographic latitude dependence on λ ,

the meridional dependence of f_oF2 on the geometry of the Earth’s magnetic field:

$$P_{jk}(\lambda, \theta) = (\sin \chi(\lambda, \theta))^j (\cos \lambda)^k, \quad (4)$$

where $\chi(\lambda, \theta)$ is the modified dip latitude introduced by Rawer [1963] for optimal global F peak mapping:

$$\chi(\lambda, \theta) = \arctan \frac{I(\lambda, \theta)}{\sqrt{\cos \theta}}. \quad (5)$$

Here $I(\lambda, \theta)$ is the true magnetic dip angle at a height of 350 km over location (λ, θ) . The $(\sin \chi)^j$ term is frequently called “geomagnetic correction,” responsible for placing the Appleton anomaly of ionization around the geomagnetic equator, rather than the geographic equator. With this organization of the spherical expansion, the first term in equation (3) represents the main meridional variation of f_oF2 as a power series expansion over $\sin \chi$. For additional compactness of the CCIR-67 set of coefficients, higher degrees of expansion k are truncated to smaller orders $J(k)$, as further detailed by ITU [2009].

[8] In summary, 1 day of the global f_oF2 distribution requires 13 diurnal \times 76 spherical = 988 coefficients C_{ijk} . The total number of stored coefficients that are used by the CCIR-67 model to obtain f_oF2 for any given time and location is 988×12 months \times 2 levels of solar activity, or 23,712 coefficients. When universal time t and location (λ, θ) are specified, the CCIR-67 model uses t to obtain the set of 988 coefficients C_{ijk} interpolated to the specific level of solar activity and day of the month, and then uses equations (2)–(5) to compute 13 coefficients A_i that enter equation (1) to obtain the f_oF2 value.

3. Assimilative IRI Requirements

[9] The IRI-RTAM is expected to match the measurements where they are available within the uncertainty bounds of the measurement and the model. In order to represent sensor-populated areas such as Europe and South Africa, IRI-RTAM has to maintain sufficiently fine spatial resolution of computed corrections, which translates to high orders of spatial expansion representation. In turn, higher expansion orders will complicate the task of representing corrections over the areas not covered by data, where unconstrained expansion of such higher order becomes prone to numerical artifacts (e.g., oscillations or other behavior incompatible with the system’s physics). The assimilation task therefore needs a suitable compromise between IRI-RTAM being true (close to data) and being reasonable (close to the expected physical behavior of the system).

[10] The need to constrain the spatial expansion in the areas of missing data was realized early in the development of the CCIR-67 global f_oF2 maps; Jones and Gallet [1962] added so-called “screen points” in the ocean regions for stability of expansion by “borrowing” averaged data from similar areas at different longitudes. Later Rush et al. [1989] revised the original extrapolation scheme by modeling the anticipated f_oF2 behavior over the areas of missing data using a model of the neutral wind transport; the resulting f_oF2 model is known in the literature as URSI-88. Similar

approaches were reinvented in other scientific fields, creating the art of the “mixed models” [e.g., *McCulloch and Searle*, 2000], whose concept is to borrow missing data from similar independent observations or physics-based simulations of the system state. If such phantom data are not brought into the model, unconstrained expansion is likely to lead to unreasonable oscillations and runaway values of the fitting solution [e.g., *Reithinger et al.*, 2008].

[11] Research has shown that simple interpolation schemes of the data/model mismatches to other locations on the globe beyond the spatial correlation radius of ~ 500 – 1500 km are hazardous [e.g., *McNamara and Wilkinson*, 2009; *McNamara et al.*, 2010, and references therein]. This research suggests that a better approach is to fade the calculated data/model mismatch as the distance from the measurement location increases. *Pezzopane et al.* [2011] studied weight functions of varying steepness of attenuation with distance away from the sensor sites and their effects on the *foF2* maps. They demonstrated that fading must be done gradually in order to avoid density discontinuities that will in turn trigger anomalous propagation artifacts in ray-tracing algorithms.

[12] Smoothness of the spatial model representation is an important criterion of assimilation in order to ensure reasonable and continuous 3-D density distributions. *Fridman et al.* [2009] described a GPS-TEC based Ionospheric Inversion (GPSII) assimilative system, in which the ionospheric density reconstruction is a nonlinear recursive optimization process that minimizes a cost function designed to guarantee smoothness of the solution within the error bounds of available measurements. GPSII uses the IRI-2007 ionospheric density profile as one of the options for the initial background ionospheric state that is then iteratively modified into agreement with available measurements. In such an approach, the background model assures the retention of well-documented ionospheric features, and its modifier function is determined through optimization. The challenge of smoothly transforming the background IRI density profile into matching observations is also addressed in the Electron Density Assimilative Model (EDAM) by *Angling and Khattatov* [2006]. Both EDAM and GPSII implemented inertia into their assimilation calculations that gradually bring the ionospheric specification back to the background definition if the sensor data are missing.

[13] Our review of the assimilation approaches revealed another important criterion: a consistent and smooth *timeline* of the IRI-RTAM ionospheric specification, free from short-lived artifacts of time scales below 1 h that can arise from the assimilation of noisy sensor data. One of the major contributors to the errors of *foF2* (or *NmF2*) and *hmF2* measurements is the automatic scaling of ionograms, or “autoscaling” [*Wilkinson*, 1998], a hard problem requiring an intelligent system approach to replicate the human capability of interpreting remote sensor images of the ionosphere. While no ideal solution to the quality issues of the ionogram autoscaling is in sight, assimilative models can benefit most from a statistical description of the confidence and uncertainty of the real-time autoscaled data [*Galkin et al.*, 2008].

[14] The assimilation quality requirements preclude direct use of the current sensor data to “spot correct” the monthly average specification within a radius of spatial correlation from the sensor locations. Such spot-corrected model, when

viewed in a time progression, can produce short-term artifacts caused by occasional errors and gaps in data. One approach with proven robustness to autoscaling errors is based on the evaluation of the effective solar activity index, R_{eff} or IG_{eff} , that provides the best instant fit of the IRI *foF2* map to the observations [*Houminer et al.*, 1993; *Bilitza et al.*, 1997]; occasional autoscaling errors at sensor sites affect the R_{eff} evaluation only insignificantly. This “effective solar index” technique has proved successful for regional modeling [e.g., *Zolesi et al.*, 2004; *Tsagouri et al.*, 2005; *Pezzopane et al.*, 2011], but is not appropriate for global modeling since solar and magnetospheric inputs may affect different regions of the globe differently.

4. Assimilative Global Empirical Modeling for IRI

4.1. Morphing Approach to Assimilation

[15] Real time measurements of *foF2* and *hmF2* remain scarce and are prone, in various degrees, to inaccuracies of the applied technique, instrumental limitations, and automatic data processing. Among multiple sources of F2 peak data, vertical HF sounding with ionosondes provides the most reliable and abundant stream of measurements with a long record of *foF2* and *hmF2* data at cadences of 1 h or better. Currently the continually growing GIRO is one of the prime suppliers of real-time ionogram-derived F2 peak data. We envision our task as updating the classic IRI electron density distribution with available GIRO data while preserving the overall integrity of its renowned representation of typical ionospheric features. Additional potential ionospheric data resources are discussed in section 4.3.5.

[16] RTAM will implement a fundamentally new assimilation scheme in which the IRI global maps are transformed into agreement with observational data by adjusting the coefficients C_{ijk} of the diurnal/spherical expansion. In this approach, the assimilated model is still described by the same IRI formalism, only that the adjusted model values now better match all available observations. We call this RTAM transformation *morphing* reflecting its concept similarity with audio timbre morphing [e.g., *Haken*, 1992], a class of techniques for blending two sounds via manipulating them in the spectral domain, rather than directly mixing them in the time domain. RTAM morphs individual harmonics of the maps rather than adjusting the map values themselves.

[17] Morphing takes the optimal place between assimilation techniques that match the background model with only latest available data prior to time t and long-term inert algorithms averaging days of historic data: it analyzes a sliding *24 h history* window of differences between model and sensor data to obtain the transformed set of coefficients of diurnal/spherical harmonics. The cartoons in Figure 3 illustrate the effect of “spot correction” (instant match) and “morphing” (24 h window) on the monthly average climatology model (dashed line) for the extreme case of only two, widely spaced sensors. The expected assimilation outcomes are shown for a meridional crosscut through the daytime ionosphere with the Appleton anomalies, and the star symbols correspond to *foF2* measurements in the northern and southern hemispheres. The spot correction technique adjusts the model values in the vicinity of available sensor locations

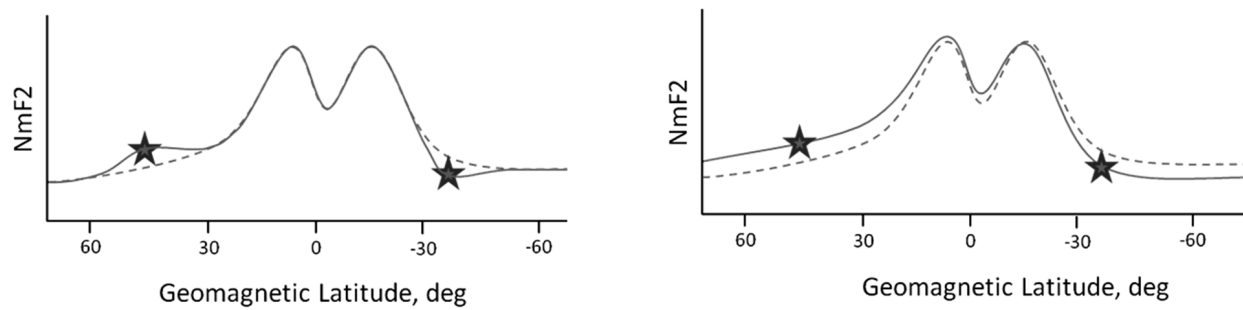


Figure 3. Cartoons illustrating two different assimilation approaches applied to a meridional cross section of f_oF2 . Star symbols indicate measured values of f_oF2 , dashed lines correspond to the standard IRI climatology, and solid lines represent the assimilation results. (left) The “spot correction” introduces artificial gradients near the data station avoided by the (right) “morphing” approach.

(Figure 3, left) producing, for this example, a depression in the southern hemisphere and a bulge in the northern hemisphere. Without a suitable temporal analysis window, such updating rule will be sensitive to data noise and gaps, resulting in occasional “pop-ups” of short-lived artifacts. Modern instant match assimilation techniques such as EDAM and GPSII make use of data error protection algorithms that involve a sliding window analysis to determine if the sensor value shall be questioned. Our morphing technique, discussed in detail below, smoothly modifies the diurnal IRI specification into matching the 24 h history of data (Figure 3, right), resulting in an IRI-like ionospheric specification that preserves the features of the original model gradients. Because of the sliding window analysis, the next assimilation calculation will be a smooth transition in time, free from short-term artifacts.

4.2. Correcting the Expansion Coefficients

[18] The proposed morphing technique first retrieves the set of 988 coefficients C_{ijk} for use in equations (2)–(5) from the stored set of coefficients and then computes 988 corrections ΔC_{ijk} that make the resulting global diurnal IRI specification better match the available 24 h history of measurement data at sensor sites. Because the corrections to the IRI coefficients will be obtained using a 24 h sliding window of measurements, the overall scheme is less susceptible to sensor data quality and availability issues that were responsible for the short-term artifacts in past attempts to build assimilative models.

[19] The corrections ΔC_{ijk} can be evaluated at the cadence of the incoming measurement data, typically 15 min for GIRO data, for simple and immediate dissemination to the IRI end users. Another advantage of such approach is that the task of interpolating data gaps in both time and space becomes easier: whereas unknown values cannot be filled in without physical understanding of the processes governing the modeled characteristic, missing information about differences between model and data can be reasonably provided by assuming a gradual controlled return to the background model.

4.3. Physics-Based Interpolation Approach

[20] The task of deriving a new set of 988 expansion coefficients C_{ijk}^* that minimize the cumulative difference between the model and data values at 40 locations \times 96 times = 3840 points

can be solved using various iterative optimization techniques. This paper describes a physics-constrained interpolation method that adds phantom points in order to keep the expansion physically reasonable and free from side effects, similarly to the original approach taken by the CCIR-67 and URSI-88 development teams.

4.3.1. Diurnal Expansion

[21] The first step in evaluating the corrections to the harmonics in equation (3) is to obtain the diurnal harmonics of the f_oF2 differences $\{\text{data} - \text{model}\}$ at ionosonde locations contributing their real-time data to the GIRO database [Khmyrov *et al.*, 2008]. This requires continuous buffering of the 24 h history of f_oF2 observations for each sensor site and repeated runs of the sixth-order diurnal harmonic expansions of the $\{\text{data} - \text{model}\}$ differences using the same formula as the CCIR-67 and URSI-88 models. Figure 4 illustrates this process by showing the f_oF2 data for Eglin, Florida on 1–2 September 2011 (solid line), the IRI monthly diurnal median of f_oF2 for September 2011 (dashed line), and the f_oF2 time series obtained using the corrected coefficients $A_i + \Delta A_i$ of the diurnal harmonics (circles). The table included in Figure 4 enlists values of 13 coefficients A_i of the diurnal expansion (equation (1)) used in the standard IRI (the left column), the corrections ΔA_i calculated using the $\{\text{data} - \text{model}\}$ differences (middle column), and the modified coefficients $A_i + \Delta A_i$ used for RTAM (right column).

[22] The diurnal harmonic expansion has the clear advantage of being robust to ionogram autoscaling errors (as in Figure 4 at 23:30 UT and 10:00 UT). It is also capable of smoothing out the autoscaled data jitter observed from 12 to 17 UT which, if taken at exact value, would be responsible for an unreasonable dynamic behavior of the assimilative IRI-RTAM. The harmonic expansion is able to bridge short data gaps whose time scale is well below the time constant of the expansion (4 h for the sixth order used in IRI). Such capability can be used to handle occasional single data dropouts and autoscaled records reported to have a low confidence level. Larger periods of missing data have to be filled in, however, to avoid potential oscillations in the gap.

4.3.2. Spherical Expansion

[23] Once the correction coefficients are obtained for each of the participating GIRO stations, each of the 13 correction coefficients ΔA_i of the diurnal expansion has to be presented globally using the same expansion of 76 spherical harmonics as in equations (2)–(5) in order to obtain the resulting

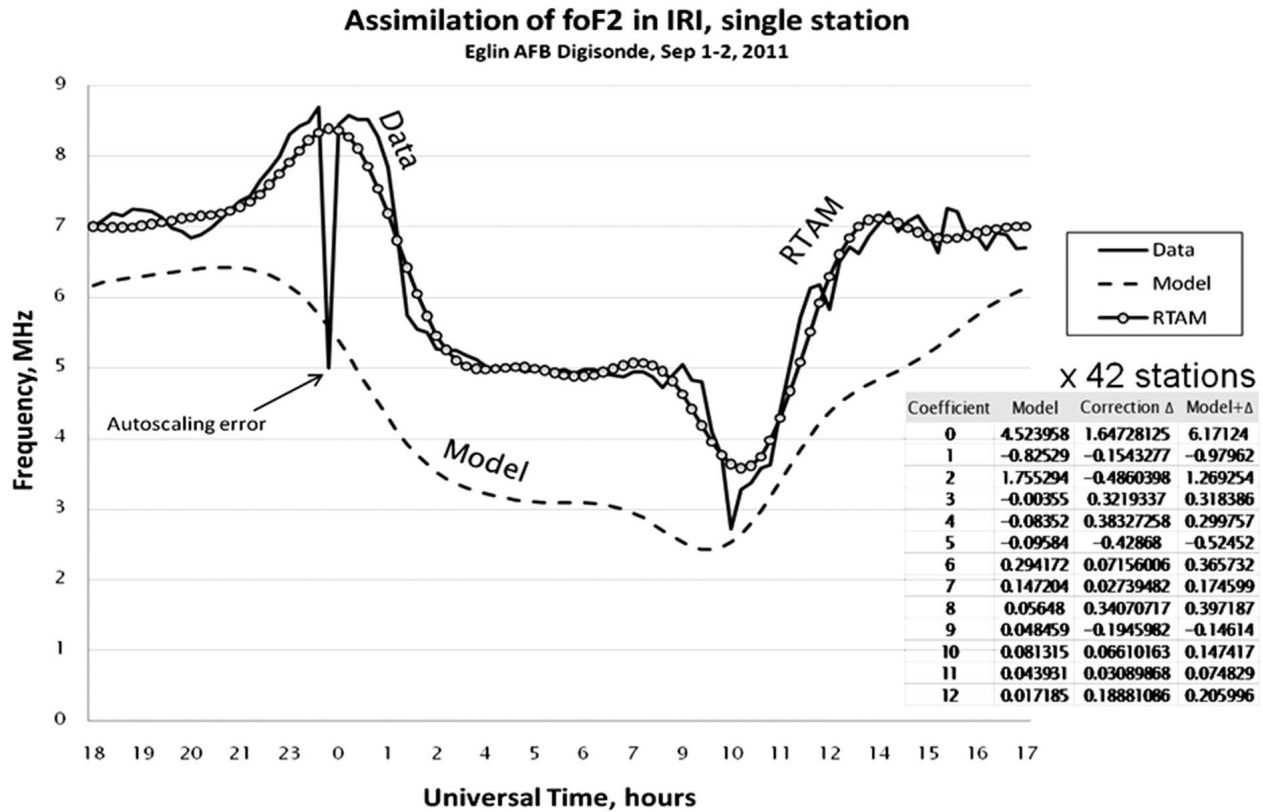


Figure 4. Illustration of RTAM assimilation concept of introducing corrections to the coefficients of the harmonic expansion: single station case, calculation of corrections to diurnal harmonics provided by URSI-88 model. Solid line indicates Eglin foF2 measurements at Eglin from 2011.09.01 18:00 to 2011.09.02 18:00. Dashed line indicates IRI climatology of foF2 for September 2011. Circles indicate IRI-RTAM assimilation by applying corrections to 13 coefficients of diurnal expansion calculated from the observed {data – model} differences.

IRI-RTAM set of 988 corrections ΔC_{ijk} . The task of evaluating spherical harmonics U_{in} , $n = 0.75$ (equation (2)), from available ΔA_i values of limited spatial coverage (<42 locations of GIRO) is underdetermined as illustrated in Figure 5. The spherical expansion of the appropriate order/degree detail has to deal with missing data between GIRO locations.

[24] Of multiple approaches to the task of spherical expansion on a sparse and unevenly spaced grid, we find the concept of filling data gaps by model-guided interpolation most appropriate, following the successful example used by the URSI-88 modeling group [Rush et al., 1989] to revise CCIR maps. Once the missing values are restored, the spatial expansion using equations (2)–(5) reduces to a much simpler case of an evenly spaced grid.

[25] As discussed earlier, it is important for the resulting IRI-RTAM specification to (1) be free from discontinuities of the plasma density distribution and (2) gradually fade corrections by returning to the background climatology with increasing distance from the data-covered areas. Figure 6 illustrates the task of filling data gaps between sensor sites that has to consider criteria 1 and 2. In order to add an interpolated value at the grid position, marked by a question mark in Figure 6, without introducing artificial gradients along any direction, the algorithm has to be aware of all

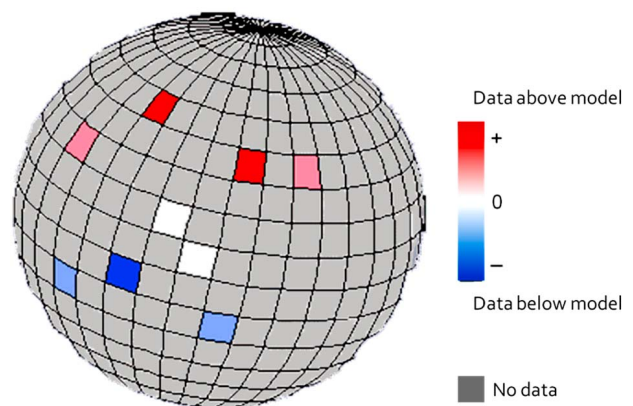


Figure 5. Simulated illustration of the underdetermined task of calculating 76 spherical harmonics coefficients for the correction term from global set of {data – model} differences. Color shades are used to show if the data value is greater (red) or lower (blue) than the model. Gray cells of the grid correspond to missing data. Current coverage of the globe by GIRO sensors is insufficient for direct evaluation of the spherical harmonics.

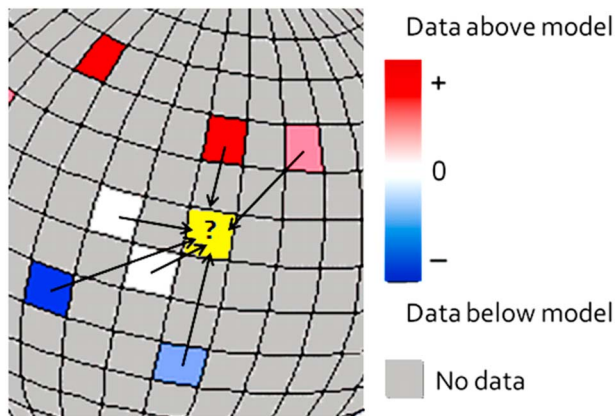


Figure 6. Filling gaps between available sensor sites (rectangles) reporting differences between model and data. Color shades are used to show if the data value is greater (red) or lower (blue) than the model. In order to avoid sharp discontinuities, each grid cell (question mark) determines its interpolated value by evaluating cumulative contributions from the neighboring cells.

neighboring grids to place the interpolated value as a weighted sum of their contributions. Additionally, for IRI-RTAM to gradually return to the background climatology specification in the areas of no data coverage, these contributions have to attenuate with distance from the sensor site. Analysis of Figure 6 and these considerations led us to an analogy with the artificial neuron and the collective dynamic behavior of the artificial neural networks. Neural networks for spatial interpolation were pioneered by *Pariente and Laurini* [1993] and since then have become an integral part of the geomatics arsenal; they proved superior in representing spatially continuous “field” variables to other classes of interpolation techniques such as Kriging or spline smoothing [Pariente, 1994]. We also found intriguing the capability of certain neural network topologies to involve additional constraints into the process of interpolation in order to reflect the presence of morphological boundaries and to account for data uncertainty, as further discussed below.

4.3.3. Neural Network Optimizer for Spherical Extrapolation

[26] Discovery of the neural doctrine has spawned a large number of computational schemes to replicate certain

intelligent functions of the brain. The doctrine describes the brain as a dynamic system made up of interconnected units, neurons, whose iteratively evolving process takes the system from its initial state to a stable final state. The neural network optimizer (NNO) for the assimilative IRI-RTAM employs a feedback recurrent Hopfield neural network [Hopfield, 1982] best known for its capability to implement functions of the human memory and early vision systems. The Hopfield networks are different from so-called feed-forward neural networks, known for their superior inductive bias, that are used for supervised modeling. The NNO for the assimilative IRI-RTAM does not have input/output layers like the feed-forward networks do, and does not use supervised training to learn known data patterns. The evolving NNO dynamic is governed by a classic collective neuron update rule [McCulloch and Pitts, 1943]:

$$Q_i = g \left(\sum_{j \neq i} V_{ij} Q_j \right) \quad (6)$$

where Q_i is the new neuron state, Q_j are states of other neurons in the network, V_{ij} are synaptic weights that regulate the strength of influence of neuron j on neuron i , and g is an auxiliary function provided to control the evolving process. On the microscopic level, each neuron decides its new state by evaluating the summary influence of other neurons of the network. Conceptually, such neuron behavior matches our interpolation task very well: each of the grid cells in Figure 6 decides its new value depending on the weighted sum of values from all other cells. In the simplest case, the weights V_{ij} can be designed to implement the proximity principle of gestalt [Rock and Palmer, 1990], i.e., attenuate contributions from more distant cells of the grid.

[27] The interpolation process with the aid of a feedback neural network optimizer starts with initializing the “anchor” grid cells where the data – model correction value is available and then lets the NNO evolve all grid cells to the self-consistent optimized state, as illustrated in Figure 7. The anchor neurons do not change their state during the evolving process.

[28] The dynamic behavior of NNO is conveniently described in terms of the energy function of the network that is shown to always decrease with each evolving step:

$$E(t) = -\frac{1}{2} \sum_{i \neq j} \sum_j V_{ij} Q_i(t) Q_j(t) \quad (7)$$

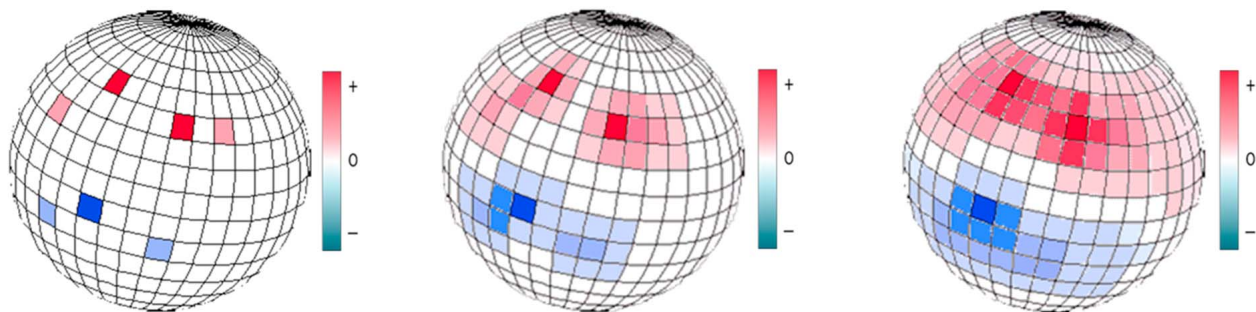


Figure 7. Neural network optimizer evolving into its stable state. (left) Initial network state with anchor neurons at GIRO sites initialized to the actual {data – model} differences. (middle) NNO state during its evolving process. (right) Final stable state showing all cells arrived at a self-consistent state.

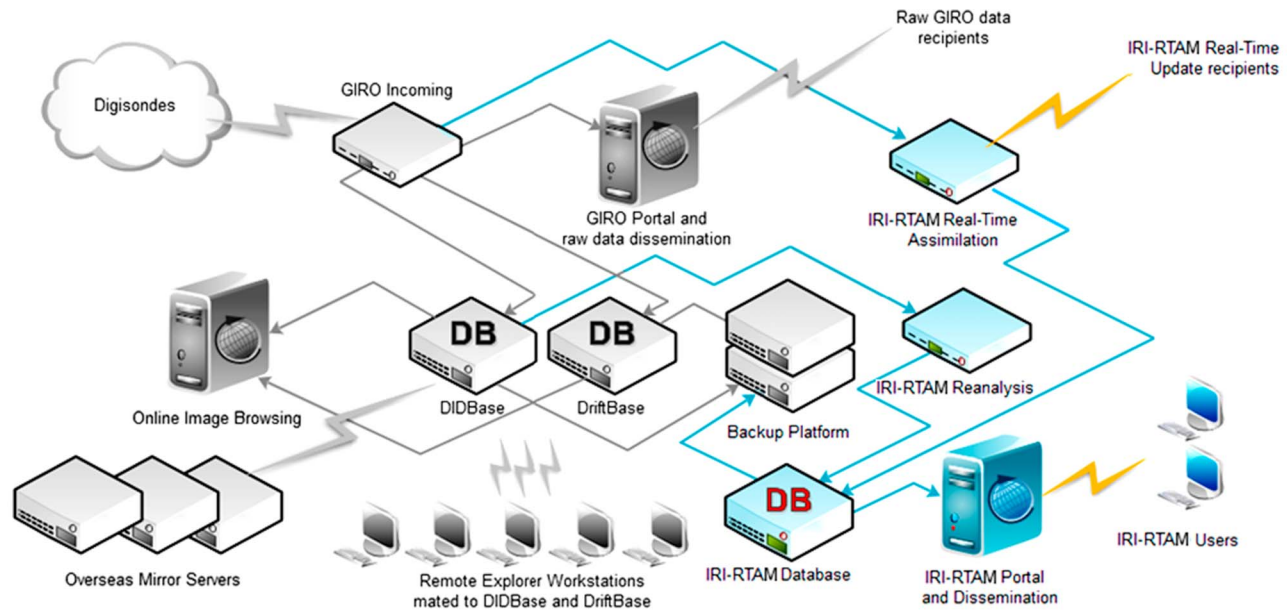


Figure 8. Computer infrastructure of Global Ionospheric Radio Observatory with additional platforms for IRI-RTAM real-time assimilation, reanalysis, and dissemination of updated ionospheric specification.

The NNO dynamic evolving process results in the neural network arriving in its global minimum of the energy function. Synaptic weights V_{ij} are calculated for pairs of interacting neurons using a suitable function that implements the proximity principle that is needed to fade the corrections outside the areas of GIRO coverage. In the simplest approach, V_{ij} can be made inversely proportional to the distance ρ_{ij} between grid cells, $V_{ij} = 1/\rho_{ij}$. A better algorithm can use the climatology IRI specification to estimate how quickly the V_{ij} have to attenuate in the given direction between locations i and j . More complex schemes of synaptic weight engineering for IRI-RTAM can be devised to identify and preserve large-scale features of storm-enhanced ionospheric plasma, such as the plumes and tongues of ionization [Foster *et al.*, 2005], that can be inferred from GIRO fragmentary data or imported from alternative data resources describing, for example, the convection flow cell pattern in the polar ionosphere. Such V_{ij} calculation schemes can employ principles of colinearity/cocircularity to identify salient features from their fragments [Wersing *et al.*, 2001; Galkin *et al.*, 2008], or introduce static patterns of limited neuron mobility into the evolving process.

[29] Once the network arrives at its global energy minimum state (Figure 7, right), the process of restoring the full specification of data – model diurnal harmonic from its given fragments is complete, and the spherical expansion using the CCIR/URSI-88 formalism can be applied to calculate the correction factors ΔC_{ijk} .

[30] McKinnell and Oyeyemi [2009] reported successful implementation of the feed-forward neural network model, different from the recurrent Hopfield optimizer for IRI-RTAM, in the task of describing the average global f_oF2 behavior at various levels of solar and geomagnetic activity. Feed-forward neural networks have proved an efficient nonlinear predictive modeling tool because of their ability

to extract from specifics a generalized knowledge about the system. In contrast, the IRI-RTAM task is to describe the specifics of the ionospheric conditions by revising the generalized knowledge using current sensor data.

4.3.4. Use of Autoscaled Data Uncertainty

[31] The ARTIST-5 autoscaling software of Digisonde ionograms [Galkin *et al.*, 2008] reports the uncertainty of the autoscaled f_oF2 values that is derived from a statistical analysis of manual – autoscaled differences in scaled ionogram traces. The uncertainty measures are used in the assimilation process by allowing the anchor neurons change their state within the uncertainty bounds.

4.3.5. Additional Data Sources

[32] As described, the assimilation technique accepts measured f_oF2 values from ground-based ionosondes or other instrumentation. For the task of building the real-time extension of the IRI, we consider GIRO as the main public provider of the real-time f_oF2 measurements. Efforts are underway for GIRO to start accepting real-time data from non-Digisonde observatories. The CCIR-67 formalism requires evaluation of corrections to 76 coefficients of spherical expansion. With current GIRO capability of 30–40 real-time feeds, the assimilation task is clearly underdetermined, but the trend in ionospheric diagnostics suggests enhanced data coverage in the foreseeable future. For example, real-time data from planned topside ionospheric sounders will drastically reduce the scarcity of f_oF2 data, especially in the ocean areas.

4.4. Assimilation of Other Ionospheric Characteristics

[33] The concept of diurnal/spherical harmonic expansion is used in IRI to hold empirical maps of peak characteristics f_oF2 and $hmF2$, as well as the profile shape parameters $B0$, $B1$, and $D1$. While our technique description was specific to the assimilation of measured f_oF2 data, the other profile

characteristics can be adjusted using a similar approach, different only by the number of coefficients in the expansions.

5. Rapid Dissemination of IRI-RTAM Specifications by GIRO

[34] The compactness of the IRI ionospheric specification allows simple practical solutions for rapid dissemination of the IRI-RT results that may be accomplished by additional GIRO computer infrastructure (Figure 8). A sliding 24 h window of incoming ionosonde data, currently buffered by the GIRO Incoming Platform, will be transferred to the dedicated real-time IRI-RTAM Assimilation Platform for calculation and output of corrected coefficient sets for the IRI-RTAM Database Platform at a nominal 15 min cadence. Publishing of the real-time and retrospective IRI-RTAM results will be done via a web portal and dissemination computer. The existing Digital Ionogram Data Base (DID-Base) of GIRO [Khmyrov *et al.*, 2008] can also be used for reanalysis of previous time periods using updated or alternative assimilation techniques.

6. Summary

[35] New assimilation techniques “update” the IRI electron density distribution while preserving the overall integrity of its typical ionospheric feature representations. Assimilation of the real-time GIRO data can improve the IRI capability to represent ionospheric responses to various short-term events observed during periods of storm activity or the impact of gravity waves coupling the ionosphere to the lower atmosphere. Our technique calculates the corrected coefficients for the spherical/diurnal expansion used by the CCIR-67/URSI-88 model to specify the global f_oF_2 maps, and similarly the maps for all other IRI profile parameters. The sets of corrected coefficients can be produced as frequently as every 15 min and they can easily be disseminated by GIRO using real-time IRI-RTAM servers.

[36] **Acknowledgments.** Eglin Digisonde data have been provided via agreement between the U.S. Air Force Weather Agency (AFWA) and the Digital Ionogram DataBase (DIDBase) of GIRO. I.G. and X.H. were, in part, supported by AF contract FA8718-06-C-0072 and by a grant from Lowell Digisonde International. D.B. was supported by NASA grant NNX09AJ746.

References

Angling, M. J., and B. Khattatov (2006), Comparative study of two assimilative models of the ionosphere, *Radio Sci.*, *41*, RS5520, doi:10.1029/2005RS003372.

Bilitza, D. (1990), International Reference Ionosphere 1990, *Rep. NSSDC/WDC-A-R&S 90-22*, 155 pp., Natl. Space Sci. Data Cent., Greenbelt, Md.

Bilitza, D. (2001), International Reference Ionosphere 2000, *Radio Sci.*, *36*(2), 261–275, doi:10.1029/2000RS002432.

Bilitza, D., and B. W. Reinisch (2008), International Reference Ionosphere 2007: Improvements and new parameters, *Adv. Space Res.*, *42*(4), 599–609, doi:10.1016/j.asr.2007.07.048.

Bilitza, D., S. Bhardwaj, and C. Koblinsky (1997), Improved IRI predictions for the GEOSAT time period, *Adv. Space Res.*, *20*(9), 1755–1760, doi:10.1016/S0273-1177(97)00585-1.

Foster, J. C., A. J. Coster, P. J. Erickson, J. M. Holt, F. D. Lind, W. Rideout, M. McCready, A. van Eyken, R. A. Greenwald, and F. J. Rich (2005), Multiradar observations of the polar tongue of ionization, *J. Geophys. Res.*, *110*, A09S31, doi:10.1029/2004JA010928.

Fridman, S. V., L. J. Nickisch, and M. A. Hausman (2009), Personal-computer-based system for real time reconstruction of the three-dimensional ionosphere

using data from diverse sources, *Radio Sci.*, *44*, RS3008, doi:10.1029/2008RS004040.

Galkin, I. A., G. M. Khmyrov, A. V. Kozlov, B. W. Reinisch, X. Huang, and V. V. Paznukhov (2008), The ARTIST 5, in *Radio Sounding and Plasma Physics, AIP Conf. Proc.*, *974*, 150–159, doi:10.1063/1.2885024.

Haken, L. (1992), Computational methods for real-time Fourier synthesis, *IEEE Trans. Signal Process.*, *40*(9), 2327–2329, doi:10.1109/78.157233.

Hernandez-Pajares, M., J. Juan, J. Sanz, and D. Bilitza (2002), Combining GPS measurements and IRI model values for space weather specification, *Adv. Space Res.*, *29*(6), 949–958, doi:10.1016/S0273-1177(02)00051-0.

Hobson, E. W. (1931), *The Theory of Spherical and Ellipsoidal Harmonics*, Cambridge Univ. Press, Cambridge, U. K.

Hopfield, J. J. (1982), Neural networks and physical systems with emergent collective computational abilities, *Proc. Natl. Acad. Sci. U. S. A.*, *79*, 2554–2558, doi:10.1073/pnas.79.8.2554.

Houminer, Z., J. A. Bennett, and P. L. Dyson (1993), Real-time ionospheric model updating, *J. Electr. Electron. Eng. Aust.*, *13*(2), 99–104.

International Telecommunications Union (ITU) (2009), ITU-R reference ionospheric characteristics, *Recomm. P.1239-2(10/2009)*, Geneva, Switzerland. [Available at <http://www.itu.int/rec/R-REC-P.1239/en>]

Jones, W., and R. Gallet (1962), Representation of diurnal and geographic variations of ionospheric data by numerical methods, *J. Res. Natl. Bur. Stand.*, *66D*(4), 419–438.

Khmyrov, G. M., I. A. Galkin, A. V. Kozlov, B. W. Reinisch, J. McElroy, and C. Dozois (2008), Exploring Digisonde ionogram data with SAO-X and DIDBase, in *Radio Sounding and Plasma Physics, AIP Conf. Proc.*, *974*, 175–185, doi:10.1063/1.2885027.

Komjathy, A., R. Langley, and D. Bilitza (1998), Ingesting GPS-derived TEC DATA into the International Reference Ionosphere for single frequency radar altimeter ionospheric delay corrections, *Adv. Space Res.*, *22*(6), 793–801, doi:10.1016/S0273-1177(98)00100-8.

McCulloch, C., and S. Searle (2000), *Generalized, Linear, and Mixed Models*, 424 pp., John Wiley, New York.

McCulloch, W. Q., and W. Pitts (1943), A logical calculus of the ideas immanent in nervous activity, *Bull. Math. Biophys.*, *5*, 115–133, doi:10.1007/BF02478259.

McKinnell, L., and E. Oyeyemi (2009), Progress towards a new global foF2 model for the International Reference Ionosphere (IRI), *Adv. Space Res.*, *43*, 1770–1775, doi:10.1016/j.asr.2008.09.035.

McNamara, L. F., and P. J. Wilkinson (2009), Spatial correlations of foF2 deviations and their implications for global ionospheric models: 1. Ionosondes in Australia and Papua New Guinea, *Radio Sci.*, *44*, RS2016, doi:10.1029/2008RS003955.

McNamara, L. F., J. M. Retterer, C. R. Baker, G. J. Bishop, D. L. Cooke, C. J. Roth, and J. A. Welsh (2010), Longitudinal structure in the CHAMP electron densities and their implications for global ionospheric modeling, *Radio Sci.*, *45*, RS2001, doi:10.1029/2009RS004251.

Pariante, D. (1994), Geographic interpolation and extrapolation by means of neural networks, paper presented at Fifth European Conference and Exhibition on Geographical Information Systems, EGIS Found., Paris, 29 March to 1 Apr.

Pariante, D., and R. Laurini (1993), Statistical spatio-temporal data interpolation and extrapolation based on neural networks, paper presented at Workshop on New Tools for Spatial Analysis, Eurostat, Lisbon, 18–20 Nov.

Pezzopane, M., M. Pietrella, A. Pignatelli, B. Zolesi, and L. R. Cander (2011), Assimilation of autoscaled data and regional and local ionospheric models as input sources for real-time 3-D International Reference Ionosphere modeling, *Radio Sci.*, *46*, RS5009, doi:10.1029/2011RS004697.

Rawer, K. (1963), Propagation of decimeter waves (HF band), in *Meteorological and Astronomical Influences on Radio Wave Propagation*, edited by B. Landmark, pp. 221–250, Academic, New York.

Rawer, K., D. Bilitza, and S. Ramakrishnan (1978), International Reference Ionosphere 78, special report, Int. Union of Radio Sci., Brussels.

Reinisch, B. W., and I. A. Galkin (2011), Global ionospheric radio observatory (GIRO), *Earth Planets Space*, *63*(4), 377–381.

Reinisch, B. W., and X. Huang (2000), Redefining the IRI F1 layer profile, *Adv. Space Res.*, *25*, 81–88, doi:10.1016/S0273-1177(99)00901-1.

Reithinger, F., W. Jank, G. Tutzy, and G. Shmueli (2008), Modeling price paths in on-line auctions: Smoothing sparse and unevenly sampled curves by using semiparametric mixed models, *J. R. Stat. Soc., Ser. C*, *57*, 127–148, doi:10.1111/j.1467-9876.2007.00605.x.

Rock, I., and S. Palmer (1990), The legacy of Gestalt psychology, *Sci. Am.*, *263*, 84–90, doi:10.1038/scientificamerican1290-84.

Rush, C. M., M. Fox, D. Bilitza, K. Davies, L. McNamara, F. Stewart, and M. PoKempner (1989), Ionospheric mapping: An update of foF2 coefficients, *Telecommun. J.*, *56-III*, 179–182.

Scherliess, L., R. W. Schunk, J. J. Sojka, D. C. Thompson, and L. Zhu (2006), The USU GAIM Gauss-Markov Kalman filter model of the

- ionosphere: Model description and validation, *J. Geophys. Res.*, *111*, A11315, doi:10.1029/2006JA011712.
- Shim, J., et al. (2010), CEDAR Electrodynamics Thermosphere Ionosphere (ETI) challenge for systematic assessment of ionospheric models, Abstract SM51A-1745 presented at 2010 Fall Meeting, AGU, San Francisco, Calif.
- Tsagouri, I., B. Zolesi, A. Belehaki, and L. R. Cander (2005), Evaluation of the performance of the real-time updated simplified ionospheric regional model for the European area, *J. Atmos. Sol. Terr. Phys.*, *67*(12), 1137–1146, doi:10.1016/j.jastp.2005.01.012.
- Wersing, H., J. J. Steil, and H. Ritter (2001), A competitive layer model for feature binding and sensory segmentation, *Neural Comput.*, *13*, 357–387, doi:10.1162/089976601300014574.
- Wilkinson, P. (Ed.) (1998), Computer-aided processing of ionograms and ionosonde records, *Rep. UAG-105*, World Data Cent. A for Sol.-Terr. Phys., Natl. Geophys. Data Cent., Boulder, Colo.
- Zolesi, B., A. Belehaki, I. Tsagouri, and L. R. Cander (2004), Real-time updating of the simplified ionospheric regional model for operational applications, *Radio Sci.*, *39*, RS2011, doi:10.1029/2003RS002936.
-
- D. Bilitza, Space Weather Laboratory, George Mason University, Fairfax, VA 22030, USA.
- I. A. Galkin and X. Huang, Center for Atmospheric Research, University of Massachusetts Lowell, 600 Suffolk St., Lowell, MA 01854, USA. (ivan_galkin@uml.edu)
- B. W. Reinisch, Lowell Digisonde International, LLC, Lowell, MA 01854, USA.